Desalination and Water Treatment 8 (2009) 100–108
www.deswater.com
1944-3994/1944-3986

Prediction of chlor-alkali's caustic current efficiency by artificial neural network; case study: A zero-gap advanced chlor-alkali cell

E. Joudaki, F. Mohammadi*, A. Yousefi, T. Mirzazadeh

Iran Polymer and Petrochemical Institute, P.O. Box 14965/115, Tehran, Iran
Tel. +98 912 146 5743; email: F.Mohammadi@ippi.ac.ir

Received 25 August 2008; accepted 17 January 2009

ABSTRACT

The progress of the membrane chlor-alkali technology resulted in a meaningful reduction of energy consumption in chlor-alkali process. In this research at first step, a zero-gap oxygen-depolarized chlor-alkali cell with a state-of-the-art silver plated nickel screen electrode (ESNS®) was employed to consider the effects of various process parameters on caustic current efficiency. The anode side anolyte pH, temperature, flow rate brine concentration and the cathode side oxygen temperature, flow rate, and the applied current density are taken as the process parameters. At the second step the pre-scaled experimental data were used to train the artificial neural networks (ANNs). The ANNs approach is used to estimate the caustic current efficiency (CCE). In the training process the back-propagation learning algorithm and several training methods were used. The minimum error was found to be that of the Levenberg–Marquardt (LM) algorithm. Excellent prediction with minimum mean square error of 1.1e−4 was made. The results showed the ANN's capability and performance for prediction of the caustic current efficiency.

Keywords: Chlor-alkali; Zero-gap advanced cell; Caustic current efficiency; Artificial neural networks

1. Introduction

Chlor-alkali energy is currently the most efficient and cleanest technology. It is accepted that the developed-membrane technology has reached the theoretical end-point on energy consumption. Attempts to reduce manufacturing costs of chlor-alkali technology have recently led to modifications of the conventional membrane electrolyzers that allow for operation at around 50% higher throughput (0.6 A/cm^2) than the standard cells. The state-of-the-art membrane reactors operate at voltages as low as 3.2 V at a typical current density of 0.4 A/cm^2 [1]. While these modifications lower the capital and maintenance costs, they result in higher cell voltages and consequently in higher energy consumption. As the energy consumption per unit weight of the products is directly proportional to the electrochemical reactor cell voltage, lowering of the cell voltage is the only route to energy savings. Over the last several years, membrane technology has been modified to the extent that no viable reduction of the cell voltage is expected from further cell modifications. However, by replacing the hydrogen-evolving cathodes in the membrane chlor-alkali cells by oxygen-depolarized cathodes (Fig. 1), the cell voltages and corresponding power consumption could be reduced by as much as 30% at 0.4 A/cm^2 [2]. In fact the oxygen-depolarized cathode has to be designed to facilitate formation of the three-phase boundaries (gas/liquid/solid) that involve oxygen, water/caustic

*Corresponding author

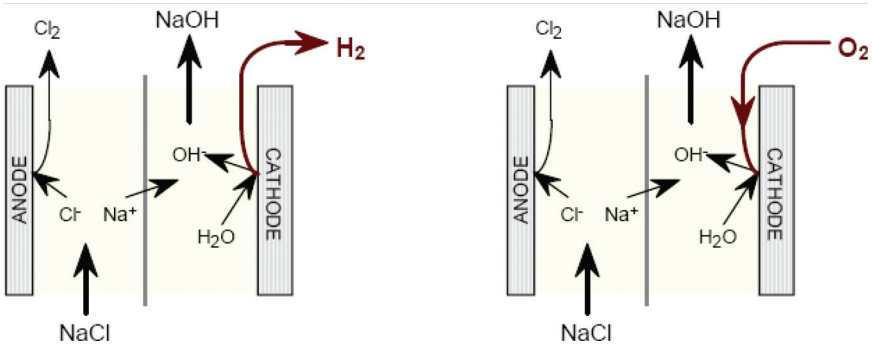

Fig. 1. The chlor-alkali cell replacing the hydrogen-evolving cathode by an oxygen-consuming cathode.

soda solution, and the catalyst particles. In addition, it has to effectively manage transport of oxygen to and caustic soda from the catalyst layer [3].

Due to the strong corrosive properties of the saturated oxygen and concentrated caustic, the chlor-alkali cells employing oxygen-depolarized cathodes are more susceptible to loose performance than the standard hydrogen-evolving cells. Therefore, the zero-gap cells were employed for this reason. In the zero-gap cells, the gas diffusion electrode remains in close contact with the ion exchange membrane. Where the oxygen and water diffuse from the gas layer side toward the electrode the cathode remains in intimate contact with the ion-exchange membrane. While the oxygen is fed to the common cathode compartment, the caustic is collected from the common cathode compartment. The hydrogen-evolving cells and the oxygen-depolarized cells also differ in the relative stability of the intermediate products of the hydrogen evolution and the oxygen reduction reactions [2,3]. The hydrogen evolution reaction does not produce any stable intermediates, i.e.

$$2H_2O + 2e^- \rightarrow H_2 + 2OH^-$$

While the oxygen reduction reaction may follow the requested four-electron path as:

$$O_2 + 2H_2O + 4e^- \rightarrow 4OH^-$$

or alternatively, according to the two-electron mechanism to generate peroxide, as:

$$O_2 + H_2O + 2e^- \rightarrow OH^- + HO_2^-$$

The peroxide eventually decomposes and produces an equivalent amount of the hydroxide and thus does not lower the overall caustic current efficiency. It is a rather troublesome byproduct, because it produces gaseous oxygen upon decomposition and may also precipitate in the highly concentrated NaOH as Na_2O_2:

$$2Na^+ + OH^- + HO_2^- \rightarrow Na_2O_2 \downarrow + H_2O$$

The sodium peroxide precipitation may cause liquid and gas flow problems by blocking the active electrode surface area and also destroying the micro porous structure of the gas diffusion electrode. The electrochemical reduction of oxygen in an alkaline environment has been the topic of many researches and the successful employment of silver [4–6] and platinum [5,6] catalysts in oxygen-depolarized chlor-alkali cathodes has already been reported. All though an oxygen-depolarized chlor-alkali cell significantly lowers energy consumption per unit weight of chlorine and caustic, simulation of the process parameters to optimize the process to get the best current efficiency is almost remained unshackled. The experimental work is very expensive and by itself cannot be used to have a clear image and understanding the process conditions and the possible problems. Therefore, it is necessary to get a model out of the limited experimental data to predict the process performance. As the major processes found in chemical engineering are nonlinear, the application of the obtained model will be of great help. The model relates input and output variables, bypassing the internal complexity of the system. Statistical models, based on regression analysis, are an example of such black box modeling. Most of these common approaches rely on linear system identification models. A different favorable alternative modeling techniques, i.e. ANN has recently found numerous applications in chemical engineering [7,8]. It should also be mentioned that neural networks had been successfully used in many technology disciplines. The ability to learn the behavior of the data generated by a system gives neural networks its versatility [8]. After a brief description of ANN, the implementation of oxygen-depolarized cathodes in a modified commercial membrane cell using ESNS® cathode will be presented. The caustic current efficiency (CCE) of the cell is studied next. Finally how to create the best ANN

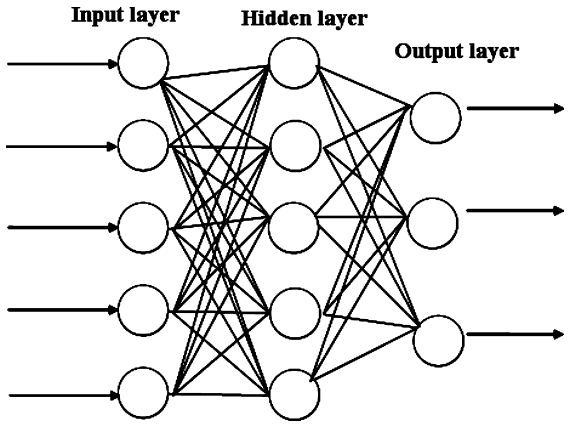

Fig. 2. A typically MLP neural network.

predictor will be described and the results are compared with the experimental data.

2. Artificial neural network (ANN)

ANN modeling is essentially a black box operation linking input to output data using a particular set of nonlinear basis functions. ANNs consist of simple synchronous processing elements, which are inspired by biological nervous systems and the basic unit in the ANN is the neuron [9]. ANNs are trained using a large number of input data with corresponding output data (input/output pairs) obtained from actual measurement so that a particular set of inputs produce, as nearly as possible, a specific set of target outputs. Thus, ANN techniques are especially useful for modeling a highly nonlinear system very well. Training consists of adjusting the weight associated with each connection (synapse) between neurons until the computed outputs for each set of data inputs are as close as possible to the experimental data outputs. In a network, each connecting line has an associated weight. Training usually begins with random valued for the weight of ANN. Then, ANNs are supplied with a set of samples belonging to problem domain to modify the values of their weights. Two important abilities of neural network are supplying fast answers to a problem and capability of generalizing the results, to make it acceptable for unknown samples [10]. There are various learning algorithms to train neural networks. One of the well-known topologies of neural networks for learning is the multi-layer perceptron (MLP), which is used for classification and estimation problems [7,8]. As shown in Fig. 2, a MLP is a neural network that has three layers, an input layer, a hidden layer, and an output layer [10].

The number of neurons in the input layer and the output layer is determined by the numbers of input and output parameters, respectively. In order to find the best ANN, the optimal number of neurons in the hidden layer has to be determined (this number will be determined based on the ANN during the training process by taking into consideration the convergence rate, mapping accuracy, etc.). Each layer consists of a series of nodes, interconnected with weights. During the learning cycle, the MLP is presented with an input pattern on the input nodes and a target pattern on the output layer. The weights are then updated so that when the network is shown the same input pattern, it gives the desired output. Each node includes an, which is a function that decides whether the neuron should glow depending on its inputs. The activation function (transfer function) is a nonlinear function. These activation functions come in many different forms, the classics being threshold, sigmoid, Gaussian, and linear function, etc. For more details of various activation functions see Bulsari [11,12].

In fact, training process requires a proper set of data, i.e. input (A_i) and target output (B_i) which during this the weights and biases of the network are iteratively adjusted to minimize the network performance function [11,12]. The typical performance function that is used for training feed forward neural networks is the network mean-squared-errors (MSE) as follows:

$$\mathrm{MSE} = \frac{1}{N}\sum_{i=1}^{N}(E_i)^2 = \frac{1}{N}\sum_{i=1}^{N}(B_i - A_i)^2 \tag{1}$$

After training (when the network is put to use), the values of the weights and the activation functions decide which nodes glowing. This type of network is feed-forward network trained with the back-propagation learning algorithm [12-14]. The back-propagation learning algorithm is based on the selection of a suitable error function, whose values are determined by the actual and predicted outputs of the network. The simplest implementation of back propagation learning is the network weights and biases updates in the direction of the negative gradient that the performance function decreases most rapidly. An iteration of this algorithm can be written as follows [12,15]:

$$P_{m+1} = P_m - l_m g_m \tag{2}$$

The model with lowest prediction error is being used as the final and optimal model.

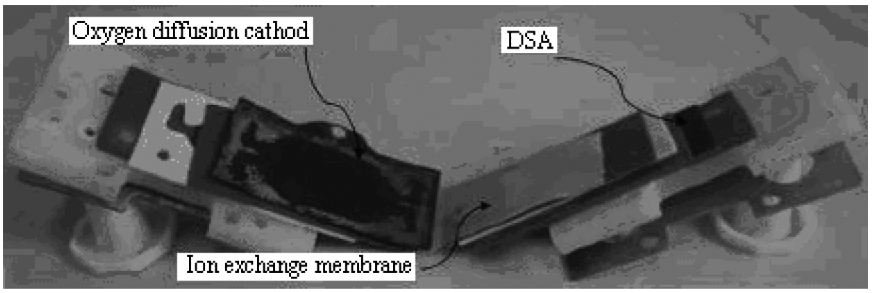

Fig. 3. Components of the membrane cell used in this study.

3. The experimental data set (materials and methods)

3.1. Chemicals used

The brine was prepared from analytical grade NaCl (Merck Inc.) using deionized water. All other chemicals used for analysis were also Analar grade.

3.2. Experimental set-up

The electrochemical cell was a divided filter-press type (Micro-flow cell, Electro cell AB, Sweden) with 10 cm^2 (3.3 cm × 3 cm) electrode area (Fig. 3) that was modified to allocate gas diffusion electrode. The cell used in this study employed a commercially available, 10 cm^2 gas diffusion electrodes (A2STD ESNS®) with a carbon-supported platinum catalyst (E-TEK Inc.). The catalyst layer contained 10% of carbon-supported (Vulcan XC-72) platinum with a total Pt loading of 0.6 mg cm^{-2}. The nickel screen side of the cathode remained in intimate contact with the carboxylic side of the ion exchange membrane (Flemion® 892, Asahi Glass Co.). The anode was a standard coated titanium plate (DSA®-Cl2). The cell flow fields were made from 2 mm Teflon. The cell performance evaluation was carried out in an ACA set-up developed in our laboratory.

Fig. 4 shows the process flow diagram of the set-up used in this study. The anolyte feed tank was heated by jacketed heater and its temperature was monitored by digital thermometer. Anolyte pH was measured by an on-line pH-meter inserted in anolyte feed tank. The anolyte was recirculated in a separate hydraulic circuit throughout the experiment by magnetic pump (Fig. 4). The overflow from the anolyte compartment of the electrolysis cell was sent to a gas–liquid separator. During electrolysis, Cl_2 gas produced was absorbed by 2 M NaOH solution in the first and the second tank, respectively. The cathode chamber was fed with oxygen at atmospheric pressure. The oxygen stream was heated and humidified by a jacketed-bubble column humidifier. The oxygen temperature and the extend of humidification were adjusted before entering into the cathode compartment. To minimize the corrosion, the cathode gas feed line was equipped with two valves that would stop the oxygen flow and replace it with nitrogen upon a power loss. Constant currents were applied to the cell and the corresponding cell voltages were measured by a multimeter. After each test, the set-up was washed thoroughly with deionized water drained and then dried. Preliminary tests showed that to create the determinable chlorine and caustic, the electrolysis run time should be at least 150 min.

3.3. Analysis

CCE was determined from titration of the sodium hydroxide samples with standardized 1.0 M HCl solution (Fisher) against phenolphthalein. The peroxide content of the NaOH solution was spectrophotometrically determined. Fresh samples of sodium hydroxide were mixed with a known amount of potassium ferricyanide solution in aqueous NaOH. The peroxide content was determined from a decrease of ferricyanide absorption at 418 nm [16]. Due to the very weak acidic properties of hydrogen peroxide (pH = 11.75 [17]), the volume of the acid used to neutralize the NaOH sample corresponding to the sum of the sodium hydroxide present in the sample and the NaOH produced as a result of hydro peroxide anion protonation [2]. Since

Fig. 4. Process flow diagram of the ACA set-up utilized.

the latter quantity was also equal to the amount of NaOH that would form because of hydro peroxide anion decomposition, the CCE quoted in this study are corrected for peroxide.

4. Simulation of the process by ANN

A great number of experiments were carried out in this study to examine the effect of each process parameter separately. In each series of experiments, only one process parameter was changed and the others were fixed. The back-propagation learning algorithm has been used in feed-forward and in single hidden layer network. The faster algorithms such as Levenberg–Marquardt (LM), gradient descent with momentum (GDM), and scaled conjugate gradient (SCG) which use standard numerical optimization techniques with learning rate and momentum constant were employed in this study. Although LM is the most efficient [11,12] in many cases, sometimes another methods can be useful or maybe the best. In the training process, anolyte pH, anolyte temperature, anolyte flow rate, brine concentration from the anode side, oxygen temperature, oxygen flow rate from the cathode side, and the applied current density process parameters were selected as the network's input (seven input nodes). The CCE (one output node) was selected as the output. Inputs and outputs are normalized between the ranges of [0–1]. Also Neurons in input layer have no transfer function. The neurons in the hidden layer perform two tasks: summing the weighted inputs connected to them and passing the result through an activation function to the output or adjacent neurons of the corresponding hidden layer (the logistic sigmoid and purelin transfer functions have been used for hidden and output layers). Also another transfer functions with various arrangements have been used but have not better performance. Each ANN has been trained with 2/3 of data set and 1/3 of data which have been used for testing the predictions of ANN. The number of hidden neurons has been systematically varied to obtain a good estimate of the trained data [12,18]. The selection criterion is the net output MSE.

5. Results and discussion

The MSE of various hidden layer neurons are shown in Fig. 5. As it can be seen in Fig. 6, the optimum number of hidden layer neurons is determined to be 8 for minimum MSE with 800 iterations (epoch). The comparison criterion was MSE between network's output and training data. After training the ANN, the models become ready for testing and evaluation by

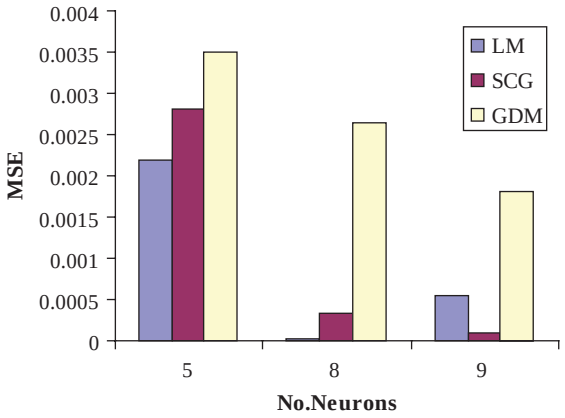

Fig. 5. Determining the optimum number of neurons for the used algorithms.

unseen data with network. The various MSE for training and testing the network is listed in Table 1. According to this table, the most suitable algorithm which provides the minimum error for the testing is found to be the LM algorithm. As the LM trained network gives much better results, it will be used for modeling the caustic current efficiency. Also as seen in Fig. 7, the relative error diagram shows the performance of the optimum ANN.

The relative error for the optimum ANN with eight neurons hidden layers and 800 epochs was shown in Fig. 7. In fact, this figure shows the quality of ANN's performance by using of relative error function between the experimental and predicted data. As shown in this figure and according to restricted error's region, the optimum ANN has good performance.

Also, as shown in Fig. 8 the ANN predicted results are very close to the process measurements (CCE) of unseen data. Also as shown in this figure, R^2 value is 0.998.

As shown in Fig. 9, the results show the good agreement between experimental and predicted data by

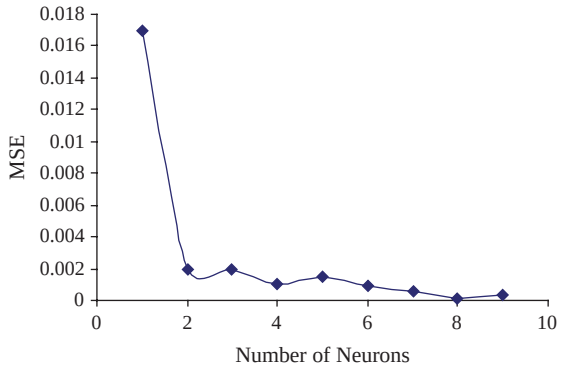

Fig. 6. The best network with 1.1e−4 MSE is obtained by 8 neurons in hidden layer.

Table 1
The MSE performance of optimum network with different algorithms

Algorithm-neurons	MSE	
	Training	Test
LM-8	0.000029	0.00011
SCG-8	0.000323	0.001910
GDM-8	0.0026481	0.032014

ANN. As shown in this figure, the CCE increases with brine concentration within the experimental range studied. At low brine concentrations, the low CCE is due to the membrane swelling and permeability. Consequently, more water is transported through the membrane yielding lower caustic concentration [19]. As could be expected, the CCE also increases with brine concentration because of decreased caustic crossover through the membrane.

As shown in Fig. 10, the results show the good agreement between experimental data and simulation by ANN. Also as shown in this figure, the CCE increases with increasing anolyte pH within the experimental range studied. It is believed that an increase in brine acidity (decrease in pH) may produce an increase in H_3O^+ flux across the membrane, which may result in a low membrane resistance, low CCE, and low NaOH concentration. However, like conventional membrane cells reported earlier [20] the chlorine current efficiency decreases with increasing brine pH due to production of hypochlorite and chlorate in anolyte at higher pH's [21].

As shown in Figs. 11 and 12, the results show the good agreement between experimental and the predicted data by ANN. The result in these figures shows

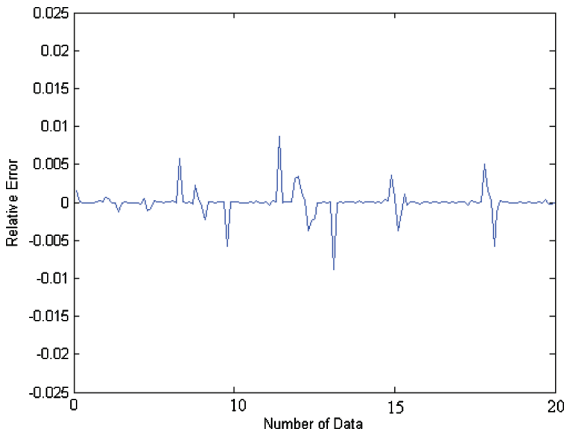

Fig. 7. A typically relative error between predicted data by optimum ANN and experimental data.

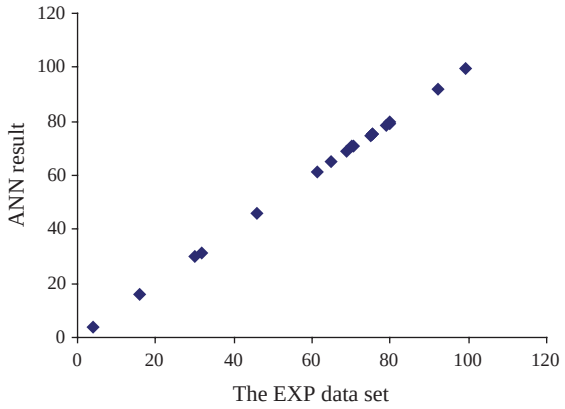

Fig. 8. The predicted CCE data by ANN vs. the experimental. Data set from lab for unseen data (with $R^2 = 0.998$).

that the CCE increases with anolyte and oxygen temperature. At low temperatures, the rate of oxygen reduction is low and this lowers the CCE profoundly [20]. Another point that should mention is that the electrical conductivity of the electrolyte is a function of concentration and temperature. At high temperatures, the high conductivity of anolyte solution lowers the cell voltage and therefore energy consumption of the chlor-alkali set-up will be low as conventional membrane cells [20]. Consequently the economic and energy factors are in favor of the technology that utilizes higher temperatures.

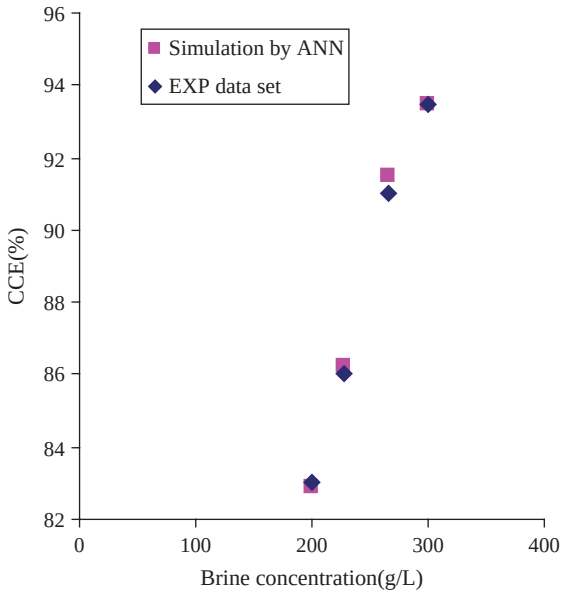

Fig. 9. A comparison between experimental data set and the predicted result (the condition is: temperature (80 °C), pH (2.5), flow rate (350 cm^3/min), oxygen: flow rate (700 cm^3/min), temperature (80 °C), and current density (0.2 A/cm^2)).

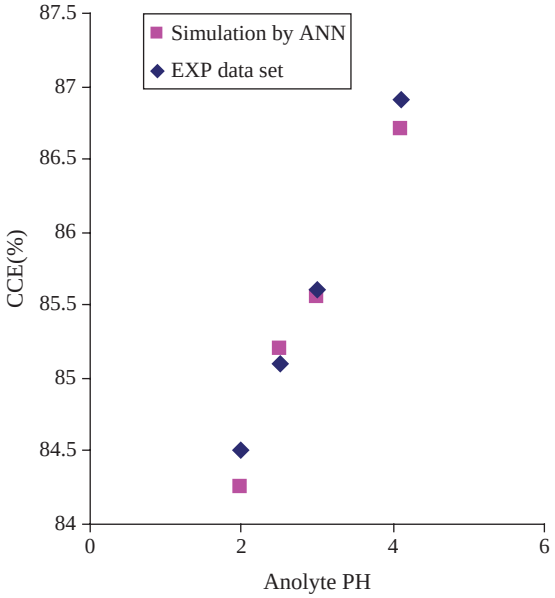

Fig. 10. A comparison between experimental data set and the predicted result (the condition is: concentration (210 g/L) temperature (75 °C), flow rate (350 cm^3/min), oxygen: flow rate (500 cm^3/min), temperature (75 °C), and current density (0.2 A/cm^2)).

As shown in Figs. 13 and 14, the results show the good agreement between experimental and predicted data by ANN.

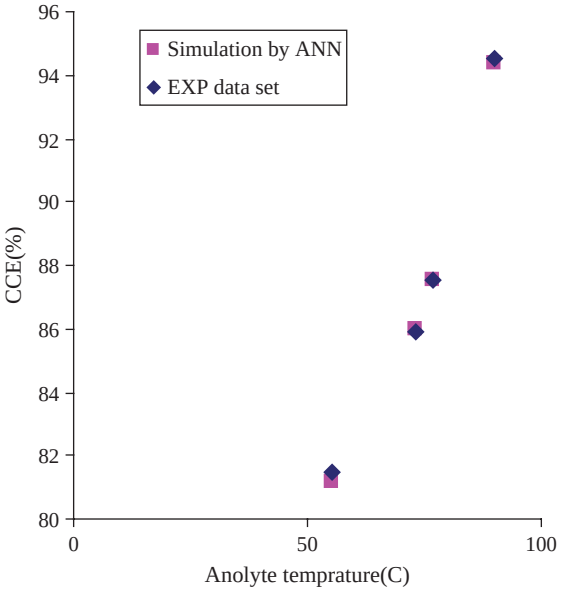

Fig. 11. A comparison between experimental data set and the predicted result (the condition is: concentration (230 g/L), pH (2.5), flow rate (350 cm^3/min), oxygen: flow rate (900 cm^3/min), temperature (75 °C), and current density (0.2 A/cm^2)).

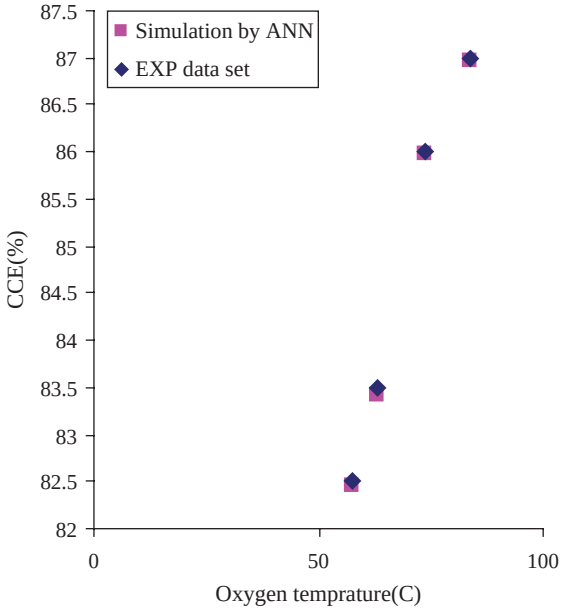

Fig. 12. A comparison between experimental data set and the predicted result (the condition is: concentration (230 g/L), pH (2.5), flow rate (250 cm^3/min), temperature (70 °C), and oxygen: flow rate (500 cm^3/min), and current density (0.2 A/cm^2)).

As shown in Fig. 13, CCE increases by increasing the anolyte flow rate. This reason may be the amount of attached Cl_2 bubbles on anodic side of the membrane and reducing those remained within anolyte

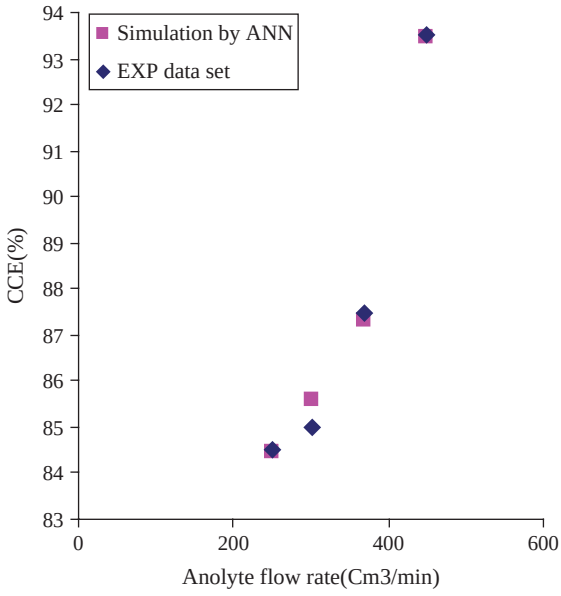

Fig. 13. A comparison between experimental data set and the predicted result (the condition is: concentration (280 g/L), pH (2.5), temperature (75 °C), oxygen: flow rate (700 cm^3/min), temperature (75 °C), and current density (0.3 A/cm^2)).

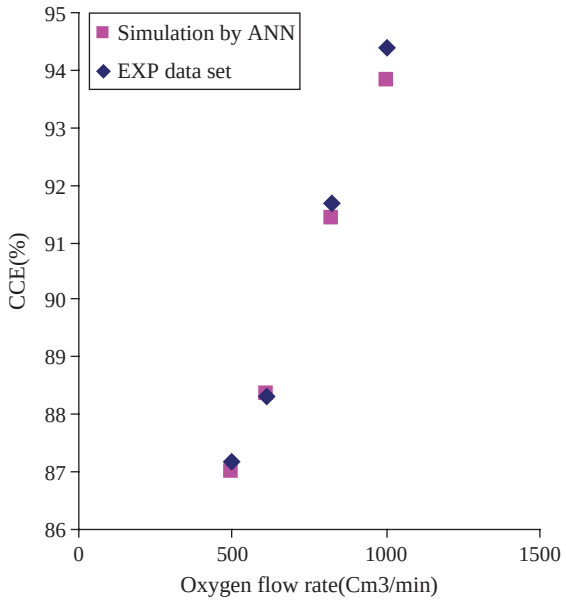

Fig. 14. A comparison between experimental data set and the predicted result (the condition is: concentration (250 g/L), pH (2.5), flow rate (400 cm^3/min), temperature (70 °C), and oxygen: temperature (70 °C), and current density (0.15 A/cm^2)).

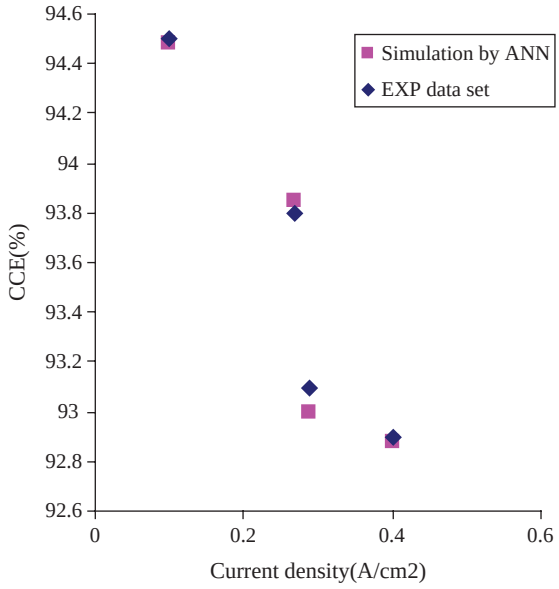

Fig. 15. A comparison between experimental data set and the predicted result (the condition is: concentration (270 g/L), pH (3), flow rate (450 cm^3/min), and temperature (80 °C), and oxygen: temperature (80 °C), flow rate (800 cm^3/min)).

[22,23]. In fact, the bubbles decrease the effective area of the membrane by blinding effects especially at low anolyte flow rates.

In addition, Fig. 14 shows that CCE increases with increasing oxygen flow rate. The increase of CCE at higher rates of oxygen flow rate most likely due to the effective caustic removal from the electrode by increasing gas flow rate. High gas velocity in the cathode chamber makes the removal of caustic from the electrode pores easier than low velocities. In very low gas velocities, we had accumulation of viscous caustic in the cathode chamber.

Also as shown in Fig. 15, the results show the good agreement between experimental and predicted data by ANN. The figure also shows that CCE is decreasing at high current densities. The effect of current density on CCE is believed to originate from the different kinetics of desirable complete 4 electron reduction and unwanted partial 2 electron reduction of oxygen, i.e.

$$O_2 + 2H_2O + 4e^- \rightarrow 4OH^-$$

$$O_2 + H_2O + 2e^- \rightarrow OOH^- + OH^-$$

In fact, the increase of current density shifts the cathode potential toward the more negative values and this phenomenon affects the relative rates of the two reactions. Higher current densities will likely decrease CCE by increasing membrane swelling, membrane permeability [19], and more significant contribution of the oxygen evolution reaction as well as membrane blinding by chlorine gas at anode side.

6. Conclusion

A modified commercial electrochemical cell with the state-of-the-art (ESNS®) cathode has been simulated to predict CCE. The paper deals with the set-up of a zero-gap advanced chlor-alkali cell and then the seven process parameters effects were studied. The experimental results revealed that CCE increases by increasing the brine concentration, anolyte temperature, anolyte flow rate, anolyte PH, oxygen temperatures, and flow rate and decreases by increasing the current density within the experimental range studied. The results showed that it is not necessary to pressurize ESNS® contrary to ELAT® [2,3] in ACA zero-gap cells. At the second step, a MLP neural network with the LM back propagation training algorithm was implemented to relate experimental data and prediction of CCE in the process. Results show a good agreement between experimental data and the predicted ANN ones. If there were industrial data for longer period of time, the ability of network could be extended to generate data in longer periods. The approach invented here needs minimum experimental data, therefore reduces time and cost of the test.

Acknowledgements

The authors are grateful to Dr. M. Baghalha from Faculty of Petroleum and Chemical Engineering of Sharif University and Dr. J. Chlistunoff from Los Alamos National Laboratory for frequent discussion and patient helps during this project.

7. Nomenclature

E	difference between target data and simulation
g	gradient
A	input data
l	learning rate
N	number of data
B	target data
P	vector of weights

References

[1] K. Yamaguchi, Chlor-alkali technologies applied in Japan, in: H.S. Burney, N. Furuya, F. Hine, K.-I. Ota (Eds.), Chlor-Alkali and Chlorate Technology: R.B. MacMullin Memorial Symposium, 196th Meeting of the Electrochemical Society, vol. 99-21, Hawaii, October, Electrochemical Society Proceedings, 1999, pp. 127-144.
[2] L. Lipp, S. Gottesfield and J. Chlistunoff, J. Appl. Electrochem., 35(10) (2005) 1015-1021.
[3] J. Chlistunoff, Advanced Chlor-Alkali Technology, Final Technical Report, Los Alamos National Laboratory, New Mexico, United States, 2004.
[4] R. Beckmann and B. Lüke, Know-how and technology—improving the return on investment for conversions, expansions and new chlorine plants, in: J. Moor House (Ed.), Modern Chlor-Alkali Technology, Proceedings of the 2000 London International Chlorine Symposium Organized by SCI's Electrochemical Technology Group, vol. 8, London, UK, 31st May–2nd June, Blackwell Science, 2001, 2000, pp. 196-212.
[5] N. Furuya and H. Aikawa, Electrochim. Acta, 45(25/26) (2000) 4251.
[6] F. Federico, G.N. Martelli and D. Pinter, Gas-diffusion electrodes for chlorine related (production) technologies, in: J. Moor House (Ed.), Modern Chlor-Alkali Technology, Proceedings of the 2000 London International Chlorine Symposium Organized by SCI's Electrochemical Technology Group, London, UK, 31st May–2nd June, Blackwell Science, 2001, 2000, pp. 114-127.
[7] G. Zahedi, A. Jahanmiri and M.R. Rahimpor., A neural network approach for prediction of the CuO-ZnO-Al_2O_3 catalyst deactivation. Int. J. Chem. React. Eng., 3 (2005) (Article A8). Available at: http://www.bepress.com/ijcre/vol3/A8.
[8] Harry Rodríguez Vallés, A Neural Networks Method to Predict Activity Coefficients for Binary Systems Based on Molecular Functional Group Contribution, Master Thesis, University of Puerto Rico, Mayaguez Campus, 2006.
[9] R. Beale and T. Jackson, Neural Computing: An Introduction, Adam Hilger, Bristol, 1990.
[10] M.T. Hagan, H.B. Demuth and M. Beal, Neural Network Design, PWS Publishing Company, Boston, 1996.
[11] H. Demuth and M. Beale, Neural Network Toolbox User's Guide, 2002.
[12] A. Moghadassi, F. Parvizian, S.M. Hosseini and S.J. Hashemi, An artificial neural network for prediction of thermodynamic properties; case study: saturated and superheated water, Chem. Technol. Ind. J., 3(2) (2008). Available at: http://tsijournals.com/ctaij/Vol_3_1/Abs07.html.
[13] J.A. Freeman and D.M. Skapura, Neural Networks, Algorithms, Applications, and Programming Techniques, Addison-Wesley, Massachusetts, 1992.
[14] S. Haykin, Neural Networks, A Comprehensive Foundation, Prentice Hall, Upper Saddle River, New Jersey, 1994.
[15] R. Gharbi, Estimating the isothermal compressibility coefficient of under saturated middle east crudes using neural networks, Energy Fuels, 11 (1997) 372.
[16] F. Aziz and G.A. Mirza, Talanta, 11 (1964) 889.
[17] L. Végvári, A. Tomposb, S. Gobülüosb and J. Margitfalvi, Catal. Today, 81(3) (2003) 517-527.
[18] G. Padmavathi, M.G. Mandan, S.P. Mitra, K.K. Chaudhuri, Neural modelling of mooney viscosity of polybutadiene rubber, Comput. Chem. Eng., 29 (2005) 1677-1685.
[19] J.T. Keating and H.M.B. Gerner, High current density operation—the behavior of ion exchange membranes in chloralkali electrolyzers, in: S. Sealey (Ed.), Modern Chlor-Alkali Technology, Proceedings of the 1997 London International Chlorine Symposium Organized by SCI Electrochemical Technology Group, vol. 7, London, UK, 4th–6th June, SCI 1998, 1997, pp. 135-144.
[20] A.A. Jalali, MSc Thesis, Iran University of Science and Technology, Department of Chemical Engineering, 2005.
[21] D. Bergner, J. Appl. Electrochem., 20(3) (1990) 716-722.
[22] J. St. Pierre and A. Wragg, Electrochim. Acta, 38(13) (1993) 1705-1710.
[23] Y. Xiong, L. Jialing and S. Hong, J. Appl. Electrochem., 22(12) (1992) 486-490.